

PatchFormer: A Versatile 3D Transformer Based on Patch Attention

Zhang Cheng^{1*}, Haocheng Wan^{1*}, Xinyi Shen², Zizhao Wu^{1†}

¹Hangzhou Dianzi University, Hangzhou China

²University College London, London UK

{zhangcheng828, wanhaocheng2022, xinyishen2018, wuzizhao}@foxmail.com, @163.com, @hdu.edu.cn

Abstract

The 3D vision community is witnessing a modeling shift from CNNs to Transformers, where pure Transformer architectures have attained top accuracy on the major 3D learning benchmarks. However, existing 3D Transformers need to generate a large attention map, which has quadratic complexity (both in space and time) with respect to input size. To solve this shortcoming, we introduce patch-attention to adaptively learn a much smaller set of bases upon which the attention maps are computed. By a weighted summation upon these bases, patch-attention not only captures the global shape context but also achieves linear complexity to input size. In addition, we propose a lightweight Multi-scale Attention (MSA) block to build attentions among features of different scales, providing the model with multi-scale features. Based on these proposed modules, we construct our neural architecture called PatchFormer. Extensive experiments demonstrate that our network achieves strong accuracy on general 3D recognition tasks with $7.3\times$ speed-up than previous 3D Transformers.

1. Introduction

Transformer has recently drawn great attention in natural language processing [5, 31] and 2D vision [6, 19, 35, 30] because of its competitive performance and superior capability in capturing long-range dependencies. Self-attention (SA), the core of Transformer, obtains an attention map by computing the affinities between self *queries* and self *keys*, generating a new feature map by weighting the self *values* with this attention map. Benefitting from SA module, Transformer is capable of modeling the relationship of tokens in a sequence, which is also important to many 3D recognition tasks. Hence, plenty of researches have been done to explore Transformer-based 3D vision architectures.

Recently, Nico et al. proposed Point Transformer [7]

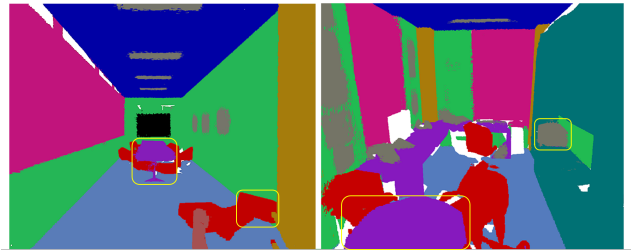


Figure 1. A large indoor scene often consists of small instances (e.g., chair and typewriter) and large objects (e.g., table and blackboard), building the relationships among them requires a multi-scale attention mechanism.

to extract global features by introducing the standard SA mechanism, which aims to capture spatial point relations and shape information. Guo et al. proposed offset-attention [8] for point cloud learning that is found to surpass the original SA module. More lately, there are more and more pure Transformer architectures [50, 34, 22] attained top accuracy on the major 3D learning benchmarks. However, they neglect the fact that the original SA module needs to generate a large attention map, which has high computational complexity and occupies a huge number of GPU memory. The bottleneck lies in that both the generation of attention map and its usage are computed with respect to all points.

Towards this issue, we propose a novel lightweight attention mechanism, namely patch-attention which calculates the attention map via low-rank approximation [46, 14]. Technically, we first segment a point cloud into patches by using the K-Means algorithm and regard the adaptive weighting center of all points in the same patch as a representative base. Then we use a product of self *queries* and self bases to approximate the global attention map, which can be obtained by computing self *queries* and self *keys*. Notably, the resulting representation of such product is low-rank and discards noisy information from the input.

The model with patch-attention is an effective network for extracting global features. However, it ignores the local neighborhood information which is also essential in 3D deep learning. For efficient local modeling, Zhang et al.

*These authors contributed equally.

†Corresponding author.

proposed PVT to build local attentions in voxels, bypassing expensive sampling and neighbor points query in point domain. Though PVT has achieved some progress, there is a problem that restricts its performance — it fails to build the attentions among features of different scales, while such ability is very important to 3D visual tasks. As shown in Figure 1, a large indoor scene often contains small instances (e.g., chair and lamp) and large objects (e.g., table), building the relationships among them required a multi-scale attention mechanism. However, the input sequence of PVT is generated from equal-sized points, so embeddings in the same layer only own features of one single scale.

To solve this issue, we present a lightweight Multi-scale Attention (MSA) block for 3D deep learning, which consists of two steps. In the first step, MSA block receives voxel grids as input, sampling boxes with multiple convolution kernels of different scales and then concatenates these voxel grids as one embedding (see Fig 5). Specifically, we propose to use the depth-width convolution (DWConv [9]) on boxes sampling because of few parameters and few FLOPs. In the second step, we incorporate 3D relative position bias and build attentions to non-overlapping local 3D window, providing our model with strong multi-scale local features at a low computational cost.

Based on these proposed blocks, we construct our neural architecture called PatchFormer (see Fig 2). Specifically, we perform the classification task on the ModelNet40 and achieve the strong accuracy of 93.6% (no voting) with $7.3\times$ faster than previous 3D Transformers. On ShapeNet and S3DIS datasets, our model also obtains strong performance (86.7% and 67.3% mIoU, respectively).

The main contributions are summarized as following:

- We propose an efficient neural architecture, termed PatchFormer, which can capably serve as a general-purpose backbone for 3D deep learning. Experiments show that our network achieves strong performance with $7.3\times$ speed-up than prior 3D Transformers.
- We present patch-attention, which can learn a more representative basis set and largely reduce the computational complexity.
- We propose a lightweight voxel-based Multi-scale Attention block, which compensates for previous architectures' disability of building multi-scale relationship.

2. Related works

2.1. Transformer for 2D Vision

Motivated by the success of Transformers in NLP [31, 26, 44, 4, 12], researchers designed visual Transformers for vision tasks to take advantage of its great attention mechanism. In particular, Vision Transformer (ViT) [6] is the first

such example of a Transformer-based approach to match or even surpass convolution neural networks (CNNs) for image classification. Later, Wang et al. [34] proposed pyramid structure into transformers, named PVT, greatly decreasing the number of patches in the later layers of the model. Liu et al. [19] proposed Swin Transformer whose representation is computed with non-overlapping local windows. Subsequently, Wang et al. [35] and Chen et al. [2] proposed CrossFormer and CrossViT to study how to learn multi-scale features in Transformers for image classification.

Inspired by the cross-scale attention used in CrossFormer and CrossViT, we present a voxel-based multi-scale attention block for 3D deep learning that combines voxel grids of different sizes to produce stronger local features.

2.2. 3D Deep Learning

Most existing 3D learning methods could be classified into two categories in terms of data representations: the *voxel*-based models and the *point*-based models. The *voxel*-based models generally rasterize point clouds onto regular grids and apply 3D convolution for feature learning [51, 24, 37]. These models are computationally efficient due to their excellent memory locality, but loss of the inevitable information degrades the fine-grained localization accuracy [28, 21]. Instead of voxelization, developing a neural network that consumes directly on point clouds is possible [23, 48, 10, 27, 43, 23, 32, 36, 47]. However, these *point*-based models naturally preserve accuracy of point location, but are generally computationally intensive.

Generally, the voxel-based models have regular data locality and can efficiently encode coarse-grained features, while the point-based networks preserve accuracy of location information and can effectively aggregate fine-grained features. In this paper, we propose PatchFormer to incorporate the advantages from two models mentioned above.

2.3. 3D Transformers

Powered by Transformer [31] and its variants [19, 6], the point-based models have recently applied SA to extract features from point clouds and improve performance significantly [8, 7, 45]. In particular, PT¹ is the first such example of a Transformer-based approach for 3D deep learning. Later, Guo et al. and Zhao et al. proposed PCT and PT² to construct SA networks for general 3D recognition tasks. Zhang et al. proposed PVT to combine the ideas of voxel-based and point-based SA and surpassed prior 3D Transformers in performance and efficiency.

However, they neglect the fact that as the size of the feature map increases, the computing and memory overheads of the original SA increase quadratically. To solve this issue, we propose patch attention to compute the relation between self *queries* and a much smaller bases, which captures the global context of a point cloud.

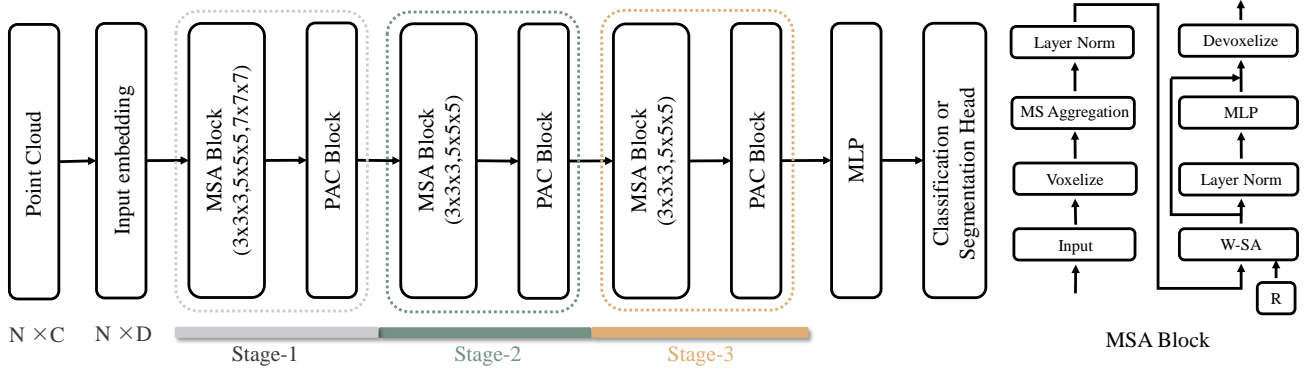


Figure 2. **The architecture of PatchFormer**: PatchFormer is comprised of three stages and each stage contains two blocks: MSA block and PAC block. A specialized head (e.g., the classification head) follows after the final stage for the specific task. **MSA block**: It first voxelizes point cloud into voxel grids, aggregating multi-scale features, and then conducts 3D window-based SA (W-SA) to capture local information. Finally, MSA block transforms voxel grids to points and feed them into PAC block. Numbers in MSA represent the size of used DWConv kernels. R denotes the relative position bias.

3. Overview

An overview of the PatchFormer architecture is presented in Figure 2. It first embeds a point cloud \mathcal{P} into a D dimensional space $F \in \mathbb{R}^{N \times D}$ using a shared MLP, where N is the number of points. We empirically set $D = 128$, a relatively small value, for computational efficiency. Later, we split our model into three stages and each stage is comprised of two blocks: Multi-scale attention (MSA) block and Patch-attention computing (PAC) block.

As illustrated in Fig 2, the MSA block first voxelizes a point cloud into regular voxel grids and then feeds them into a multi-scale (MS) aggregating module. In this module, we sample boxes using three DWConv kernels of different size and concatenate them as one embedding. After that, we limit SA computation to non-overlapping local boxes for alleviating the quadratic complexity of the original SA. Note that a LayerNorm (LN) layer is applied before W-SA module and MLP module, and a residual connection is applied after each module. Eventually, we leverage the trilinear interpolation to transform the voxel grids to points.

Like ViT [6], the PAC block treats each point as a “token” and aggregates global feature by using a patch-attention. It receives MSA block’s output as input, estimates a much more compact bases and generates global attention map upon these bases. Note that, our method reduces the complexity (both in space and time) from $\mathcal{O}(N^2)$ of the original SA to $\mathcal{O}(MN)$ where M is the number of bases. As a result, the proposed patch-attention can conveniently replace the backbone networks in existing 3D Transformers for various 3D vision tasks.

Throughout the next sections we use the following notations: the original point cloud with N points is denoted by $\mathcal{P} = \{p_i\}_{i=1}^N \subseteq \mathbb{R}^C$. In the simplest setting of $C = 3$, each point contains 3D coordinates. $F = \{f_i\}_{i=1}^N \subseteq \mathbb{R}^D$ is the

input embedding feature.

4. Method

In this section, we start by analyzing the original SA mechanism. Then we detail our novel way to define attention: patch-attention. Finally, we discuss the design of MSA block in detail.

4.1. Self-Attention

We first revisit the self-attention (SA) mechanism. The standard SA, also called scalar dot-product attention, is a mechanism that calculates semantic affinities between different elements within a sequence of data. Following the terminology in [31], let Q, K, V be the *query, key* and *value* matrices, respectively, generated by linear transformations of the input features $F \in \mathbb{R}^{N \times D}$ as follows

$$(Q, K, V) = (W_q, W_k, W_v)F, \quad (1)$$

$$Q, K, V \in \mathbb{R}^{N \times D}, \quad (2)$$

where W_q, W_k and W_v are the shared learnable linear transformation as illustrated in Figure 3.

Using the pairwise dot product $QK^T \in \mathbb{R}^{N \times N}$, then SA can be formulated as:

$$A = (\alpha_{i,j}) = \text{softmax}(QK^T), \quad (3)$$

$$F_{out} = AV, \quad (4)$$

where $A \in \mathbb{R}^{N \times N}$ is the attention map and $\alpha_{i,j}$ is the pairwise affinity between (similarity of) the i -th and j -th elements. It is apparent, that the output F_{output} is a weighted sum of V , where a value gets more weight if the similarity between the keys and values yields a higher attention weighting score.

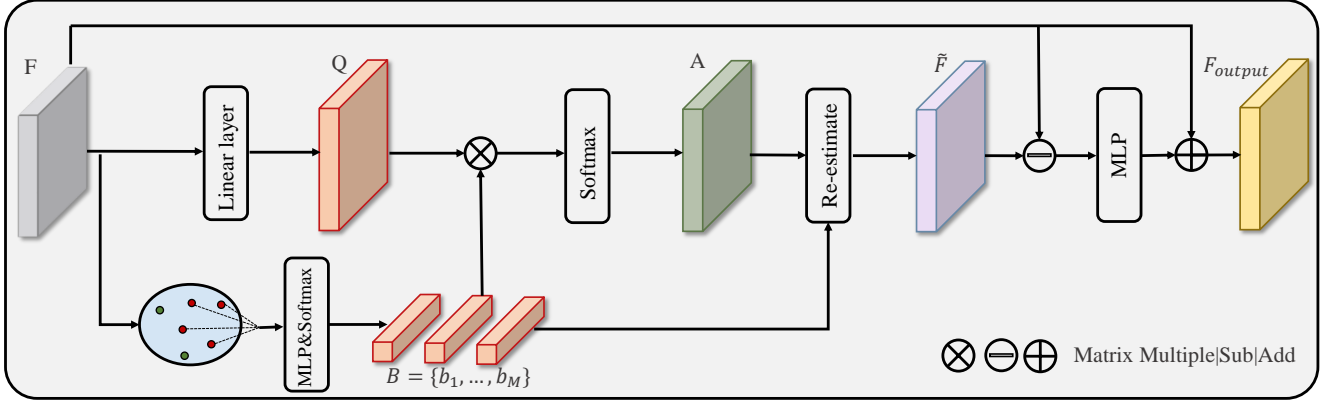


Figure 3. Architecture of PAC block (patch-attention). Patch-attention can be seen as an variant to the original self-attention to approximate global map at a lower computational cost.



Figure 4. An chair model under different transformations is shown here, the segmented patches are color-coded according to their corresponding IDs. We find bases by computing the adaptive weighting center in the same patch.

However, the high computational complexity of $\mathcal{O}(N^2D)$ presents a significant drawback to use of SA. The quadratic complexity in the number of input points makes direct application of SA to point cloud infeasible.

4.2. Patch-Attention

In view of the high computational complexity of the attention mechanism and limitations, we first propose the patch-attention method, which is an augmented version of SA. Unlike prior 3D Transformers obtain an attention map by computing affinities between self *queries* and self *keys*, our patch-attention computes the relation between self *queries* and a much smaller bases, which captures the global context of a point cloud.

For simplicity, we consider an input point cloud \mathcal{P} and its corresponding feature map F of size $N \times D$. Our proposed patch-attention is illustrated in Fig 3 which consists of two steps, including **base estimation** and **data re-estimation**. At below, we describe the proposed components in details and then discuss their connections to other recent related approaches.

Base Estimation. In this step, we estimate a compact basis set $B \in \mathbb{R}^{M \times D}$ where M is the number of bases. In particular, we use the K-Means algorithm to segment \mathcal{P} into M patches $\{S_1, S_2, \dots, S_M\}$, $M=96$, by default (see Fig 4). We define each base as b_m by aggregating the representa-

tions of all the points in the S_m , it can be described as:

$$b_m = \sum_{f_i \in S_m} w_i(\varphi(f_i)). \quad (5)$$

$$B = \{b_m\}_{m=1}^M \subseteq \mathbb{R}^D. \quad (6)$$

Here, f_i is the representation of point p_i . The transformation function $\varphi(\cdot)$ is an MLP with one linear layer and one ReLU nonlinearity. w_i is the normalized degree for f_i belonging to the S_m . We use spatial softmax to normalize each patch.

The idea of our base estimation method is motivated by MID-Net [33], a unsupervised 3D learning method for shape analysis, which uses the K-Means algorithm over-segment each shape into patches. In this way, the global shape can be approximated by the set of each patch centroid. However, we argue that such method ignores the relationships between point and other points in the same patch. In contrast, our method can adaptively adjust the contribution of all points in the same patch to the base via a data-driven way. Such adaptive adjusting facilitates to fit the intrinsic geometry submanifold.

Data Re-estimation. After estimating the bases B , we can replace K matrices with B and re-formulate Eq 3 as:

$$A = \text{softmax}(Q \cdot B^T). \quad (7)$$

where $A \in \mathbb{R}^{N \times M}$ is the attention map constructed from a compact basis set. After that, the final bases B and attention map A are used to re-estimate the inputs F . We adopt next equation to re-estimate the new F , namely \tilde{F} which can be formulated as:

$$\tilde{f}_i = \sum_{m=1}^M A_i^m \cdot b_m, \quad (8)$$

$$\tilde{F} = \{\tilde{f}_i\}_{i=1}^N \subseteq \mathbb{R}^D. \quad (9)$$

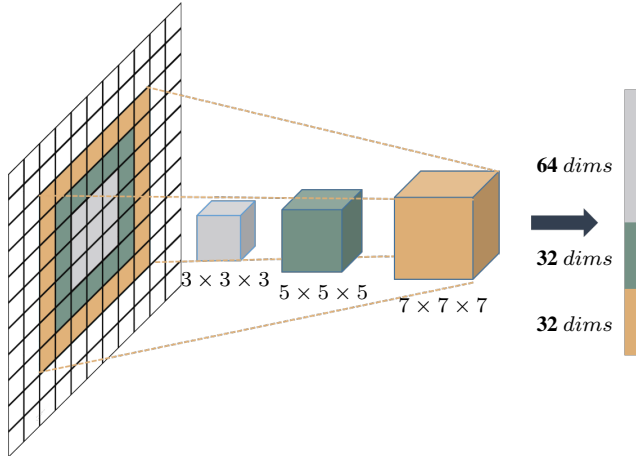


Figure 5. Illustration of multi-scale feature aggregating in MSA block on Stage-1. We note that this is a 2D example and can be easily extended to 3D cases. The input voxel grids is sampled by three DWConv kernels (i.e., $3 \times 3 \times 3$, $5 \times 5 \times 5$, $7 \times 7 \times 7$) with stride $3 \times 3 \times 3$. Each embedding is constructed by projecting and concatenating the three 3D boxes.

As $\tilde{F} \in \mathbb{R}^{N \times D}$ is constructed from a compact basis set B , it has the low-rank property compared with the input F .

Inspired by PCT [8], we calculate the difference between the estimated features \tilde{F} and the input features F by element-wise subtraction which brings our network better performance. Finally, we feed the difference into MLP layer and adopt residual connection strategy to help propagate information to higher layers. This step can be described as:

$$F_{output} = \phi(\tilde{F} - F) + F, \quad (10)$$

where $F_{output} \in \mathbb{R}^{N \times D}$ is the outputs of our PAC block and $\phi(\cdot)$ is an MLP with one linear layer and one ReLU nonlinearity.

Complexity Analysis. Compared with the standard SA module, our patch-attention finds a representative set of bases for points of a point cloud, which reduces the complexity from $\mathcal{O}(N^2)$ to $\mathcal{O}(MN)$, where M and N are the number of bases and points, respectively ($M \ll N$). Moreover, we only need to calculate K-Means algorithm once on the original point cloud \mathcal{P} and it can be accelerated in parallel by CUDA. Although the K-Means optimization has an asymptotic complexity $\mathcal{O}(NMC)$, it can be ignored in our network because M is fixed and $C = 3$, a relatively small value.

4.3. Multi-Scale Attention

In this subsection, we detail how our MSA block learns multi-scale feature representations in attention models. This block consists of two steps, including **Multi-scale feature aggregating** and **Attention building**.

Multi-scale Feature Aggregating. This step is used to generate multi-scale features for each stage. Figure 5

takes the first MSA block, which is ahead of the Stage-1, as an example. It receives voxel grids as input, sampling boxes using three kernels of different size. The strides of three kernels are kept the same so that they generate the same number of embeddings. As we can see in Figure 5, every three corresponding boxes have the same center but different scales. These three boxes will be projected and concatenated as one embedding. In practice, the process of sampling and projecting can be implemented through three DWConv layers. Like CrossFormer [35], we use a lower dimension for large kernels while a higher dimension for small kernels. Figure 5 provides the specific allocation rule in its subtable, and a 128 dimensional example is given. Compared with allocating the dimension equally, our scheme saves much computational cost while maintaining the model’s high performance. The MSA blocks in other stages work in a similar way. As shown in Figure 2, MSA blocks in Stage-2/3 use two kernels ($3 \times 3 \times 3$ and $5 \times 5 \times 5$). The strides are set as $3 \times 3 \times 3$.

Attention Building. To build the attentions among features of different scales, we attempt to conduct the standard SA on multi-scale feature map. However, the computation complexity of the full SA mechanism is quadratic to feature map size. Therefore, it will suffer from huge computation cost for 3D vision tasks that take high resolution feature maps as input, such as semantic segmentation.

To solve this shortcoming, our MSA block limits the SA computation to non-overlapping local 3D window. In addition, we observe that numerous previous works [20, 19, 38] have show that it can be advantageous to include relative position bias in SA computation. Thus we follow [19] by introducing 3D relative position bias $R \in \mathbb{R}^{V^3 \times V^3}$ as

$$F_{output} = softmax(QK^T + R)V, \quad (11)$$

where $Q, K, V \in \mathbb{R}^{V^3 \times D}$ are the *query*, *key* and *value* matrices, and V^3 is the number of voxel grids in a local box. Since the relative position along each axis lies in the range $[-V+1, V-1]$, we parameterize a smaller-sized bias matrix $\hat{R} \in \mathbb{R}^{(2M-1) \times (2M-1) \times (2M-1)}$, and values in R are taken from \hat{R} .

For cross-box information interaction, existing works [34, 19, 30] suggest to apply halo or shifted box to enlarge the receptive filed. However, the voxel grids within each Transformer block still has limited attention area and requires stacking more blocks to achieve large receptive filed. In our network, the local attention is building in multi-scale input features. Thus, we don’t need to stack more attention layers for cross-box connection or larger receptive filed.

5. Experiments

In this section, we evaluate the proposed PatchFormer for different tasks: classification, part segmentation, and

Model	points	OA	Latency
	OA<92.5		
PointNet [23]	16×1024	89.2	13.6
PointNet++ [25]	16×1024	91.9	35.3
SO-Net [13]	8×2048	90.9	–
PointGrid [11]	16×1021	92.0	–
SpiderCNN [41]	8×1024	92.4	82.6
PointCNN [15]	16×1024	92.2	221.2
PointWeb [49]	16×1024	92.3	–
PVCNN [21]	16×1024	92.4	24.2
	OA>92.5		
KPCConv [29]	16×6500	92.9	120.5
DGCNN [36]	16×1024	92.9	85.8
LDGCNN [47]	16×1024	92.7	–
PointASNL [42]	16×1024	93.2	923.6
PT ¹ [7]	16×1024	92.8	320.6
PT ² [50]	8×1024	93.7	530.2
PCT [8]	16×1024	93.2	92.4
PVT[34]	16×1024	93.6	45.5
PatchFormer	16×1024	93.6	34.3

Table 1. Results on ModelNet40 [40]. Compared with previous Transformer-based models, our PatchFormer achieves the promising accuracy with $7.3\times$ measured speed-up on average.

scene semantic segmentation. Performance is quantitatively evaluated using four metrics: mean class accuracy, overall accuracy (OA), per-class intersection over union (IoU), and mean IoU (mIoU). For fair comparison, we report the measured latency and model size on a RTX 2080 GPU to reflect the efficiency but evaluate other indicators on a RTX 3090 GPU. Please refer to our appendices for more detailed network architecture and experimental results.

Implementation details. We implement the PatchFormer in PyTorch. We use the SGD optimizer with momentum and weight decay set to 0.9 and 0.0001, respectively. For 3D shape classification on ModelNet40 and 3D object part segmentation on ShapeNetPart, we train for 250 epochs. The initial learning rate is set to 0.01 and is dropped until 0.0001 by using cosine annealing. For semantic segmentation on S3DIS, we train for 40K iterations with initial learning rate 0.5, dropped by 10x at steps 24K and 32K.

5.1. Shape Classification

Data. We evaluate our model on the ModelNet40 [39] dataset. This dataset contains 12,311 computer-aided design models from 40 man-made object categories, in which 9,843 models are used for training and 2,468 models are used for testing. We follow the experimental configuration of Qi et al. [23]: (1) we uniformly sample 1,024 points from the mesh faces for each model; (2) the point cloud is re-scaled to fit the unit sphere; and (3) the (x,y,z) coordi-

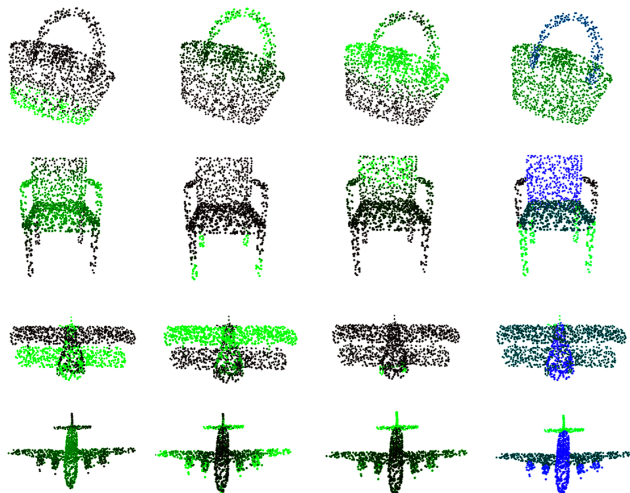


Figure 6. Attention map and segmentation results on ShapeNet. Left to right: attention maps w.r.t. three selected entries in the bases, segmentation results.

nates and the normal of the sampled points are used in the experiment. During the training process, randomly scaling and perturbing the objects are adopted as the data augmentation strategy in our experiment.

Results. The results are presented in Table 1. The overall accuracy of PatchFormer on ModelNet40 is 93.6%. It outperforms strong graph-based models such as DGCNN, strong point-based models such as KPCConv and excellent attention-based networks such as PointASNL. Remarkably, compared with existing Transformer-based models such as PT¹, PT², PCT and PVT, our model is $7.3\times$ faster, while achieving comparable accuracy.

5.2. Object Segmentation

Data. We use the large-scale 3D dataset ShapeNet Parts [16] as the experiment bed. ShapeNet Parts contains 16,880 models (14,006 models are used for training, and 2874 models are used for testing), each of which is annotated with two to six parts, and the entire dataset has 50 different part labels. We sample 2,048 points from each model as input, with a few point sets having six labeled parts. We directly adopt the same train–test split strategy similar to DGCNN [36] in our experiment.

Results and Visualization. Table 2 shows the class-wise segmentation results. The evaluation metric used is mIoU, and is given both overall and for each object category. The results show that our PatchFormer achieves the strong results with 86.7% mIoU. In addition, we randomly select three entity from B in the last layer of our network and show their corresponding attention score of all points. As we can see, each basis corresponds to an abstract concept of the point cloud and the learned attention maps focus on meaningful parts for object segmentation task as in Fig 6.

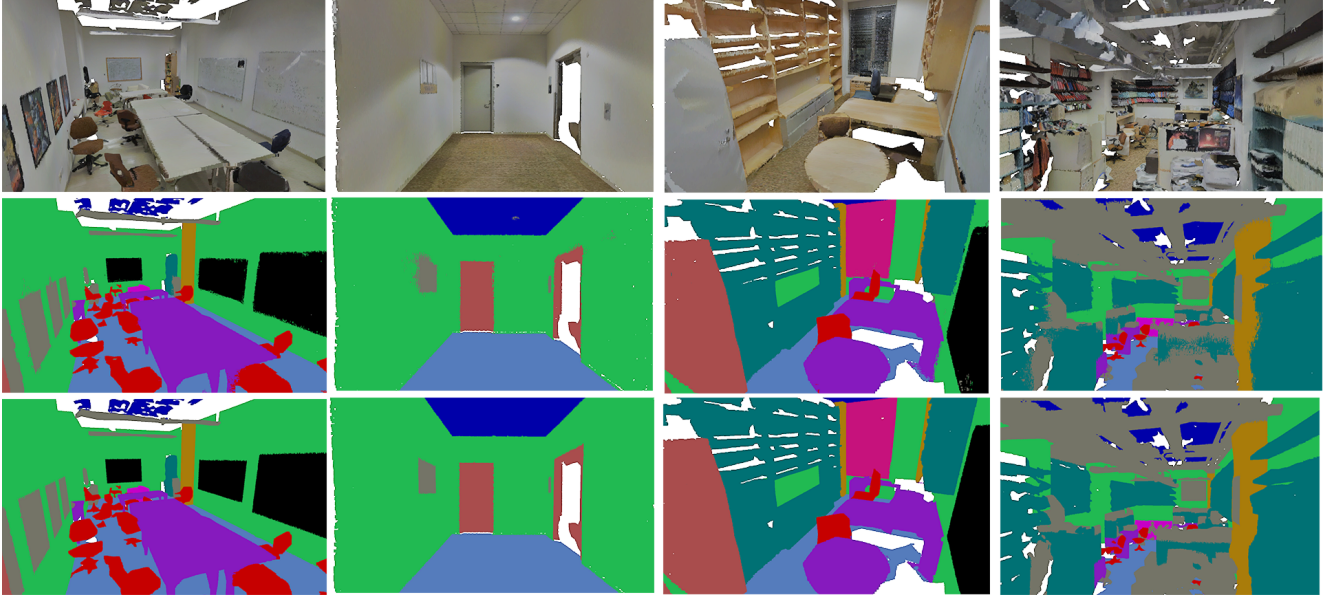


Figure 7. Visualization of semantic segmentation results on the S3DIS dataset. The input is in the top row, PatchFormer predictions on the middle, the ground truth on the bottom.

Model	mIoU	Areo	Bag	Cap	Car	Chair	Ear Phone	Guitar	Knife	Lamp	Laptop	Motor	Mug	Pistol	Rocket	Skate Board	Table
# Shapes		2690	76	55	898	3758	69	787	392	1547	451	202	184	283	66	152	5271
PointNet	83.7	83.4	78.7	82.5	74.9	89.6	73.0	91.5	85.9	80.8	95.3	65.2	93.0	81.2	57.9	72.8	80.6
P2Sequence[17]	85.1	82.6	81.8	87.5	77.3	90.8	77.1	91.1	86.9	83.9	95.7	70.8	94.6	79.3	58.1	75.2	82.8
PointASNL	86.1	84.1	84.7	87.9	79.7	92.2	73.7	91.0	87.2	84.2	95.8	74.4	95.2	81.0	63.0	76.3	83.2
RS-CNN[18]	86.2	83.5	84.8	88.8	79.6	91.2	81.1	91.6	88.4	86.0	96.1	73.7	94.1	83.4	60.5	77.7	83.6
PT ¹	85.9	—	—	—	—	—	—	—	—	—	—	—	—	—	—	—	—
PCT	86.4	85.0	82.4	89.0	81.2	91.9	71.5	91.3	88.1	86.3	95.8	64.6	95.8	83.6	62.2	77.6	73.7
PVT	86.5	85.1	82.8	88.3	81.5	92.2	72.5	91.0	88.9	85.6	95.4	76.2	94.7	84.2	65.0	75.3	81.7
PatchFormer	86.7	85.5	83.0	87.9	82.3	92.4	72.3	91.4	89.1	85.6	94.8	77.3	94.5	84.1	65.4	75.2	82.7

Table 2. Results of part segmentation on ShapeNet. mIoU means that mean Intersection-over-Union.

5.3. Indoor Scene Semantic Segmentation

Data. We evaluate our model on the S3DIS dataset [1], which contains 3D RGB point clouds from six indoor areas of three different buildings. Each point is marked with a semantic label from 13 categories (e.g., board, bookcase, chair, ceiling, and beam) plus clutter. Following a common protocol [29], we divide and sample each room into $1\text{ m} \times 1\text{ m}$ blocks, wherein each point is represented by a 9D vector (XYZ, RGB, and normalized spatial coordinates). In addition, the points in each block are sampled into a uniform number of 4,096 points during the training process, and all points are used in the test.

Results and Visualization. The results are presented in Tables 3. From this table we can see that our PatchFormer attains mIoU of 67.3%, which outperforms MLPs-based frameworks such as PointNet [23] and PointNet++ [25],

graph-based methods such as DGCNN [36], sparse convolutional networks such as MinkowskiNet [3], continuous convolutional networks such as KPConv [29], attention-based models such as PointASNL [42], Transformer-based models such as PVT [34].

Fig 7 shows the PatchFormer’s predictions. We can see that the predictions are very close to the ground truth. PatchFormer captures detailed multi-scale features in complex 3D scenes, which is important in our network.

5.4. Ablation Studies

We now conduct a number of controlled experiments that examine specific decisions in the PatchFormer design. These studies are performed on the classification and part segmentation tasks.

Number of Bases. We first investigate the setting of the number of bases. The results are shown in Table 5. The

Model	mIoU	Ceiling	Floor	Wall	Bean	Column	Window	Door	Chair	Table	Bookcase	Sofa	Board	Clutter
PointNet	41.1	88.8	97.3	69.8	0.0	3.9	46.2	10.7	52.6	58.9	40.2	5.8	26.3	33.2
PointNet++	50.0	90.7	96.4	74.1	0.0	5.7	43.5	25.3	69.2	76.9	21.4	55.6	49.3	41.8
DGCNN	47.1	92.4	97.4	76.0	0.3	12.0	51.5	27.0	64.8	68.5	7.6	43.7	29.4	40.8
PointASNL [42]	62.6	94.3	98.4	79.1	0.0	26.7	55.2	66.2	83.3	86.8	47.6	68.3	56.4	52.1
PVT[34]	65.3	91.2	98.7	86.2	0.3	34.2	49.9	61.4	81.6	89.8	48.2	79.9	76.4	54.6
MinkowskiNet [3]	65.4	91.8	98.7	86.2	0.0	34.1	48.9	62.4	81.6	89.8	47.2	74.9	74.4	58.6
KPConv [29]	67.1	92.8	97.3	82.4	0.0	23.9	58.0	69.0	81.5	91.0	75.4	75.3	66.7	58.9
PatchFormer	67.3	92.2	98.9	86.8	0.8	34.6	54.9	61.8	80.5	92.3	48.9	79.2	77.2	56.1

Table 3. Indoor scene segmentation results on the S3DIS dataset, evaluated on Area5. From this table, we can see that the proposed PatchFormer outperforms most of previous 3D models in all categories significantly,

M	ModelNet40(OA)	ShapeNet(mIoU)	Latency
32	91.54	83.92	33.25
64	92.94	85.82	33.82
96	93.62	86.72	34.32
128	93.55	86.74	35.56

Table 4. Ablation study: number of bases M in our network. We report latency on ModelNet40 dataset.

Ablation	ModelNet40(OA)	ShapeNet(mIoU)
w/o MS feature	92.85	85.22
MS feature	93.62(+0.77)	86.72(+1.50)
MLP	92.62	85.32
EdgeConv	93.10	85.89
PatchAttention	93.62	86.72
no rel. pos	93.15	86.30
rel. pos	93.62 (+0.47)	86.72(+0.42)

Table 5. Ablation study on the multi-scale feature aggregation and patch-attention on two benchmarks. w/o MS feature: all MSA block without aggregate multi-scale features. MLP: replace patch-attention with MLP layer in our architecture. EdgeConv: replace patch-attention with EdgeConv layer in our architecture. rel. pos: the default settings with an additional relative position bias term (see Eq 11).

best performance is achieved when M is set to 96. On the one hand, when the bases is smaller ($M = 32$ or $M = 64$), the model may not have sufficient context for its predictions. On the other hand, increasing M doesn't give PatchFormer much accuracy benefit but incurs a raise on latency. This also demonstrates the efficiency and effectiveness of our patch-attention.

Effect of Multi-scale feature aggregating. We conduct an ablation study on the Multi-scale feature aggregating step. From Table 5, we can see that the performance without this step on ModelNet40 and ShapeNet are 92.85%/85.22%, in terms of OA/mIoU. It is much lower than the performance with Multi-scale feature (93.62%/86.72%). This suggests that the Multi-scale feature is essential in this set-

ting.

Impact of Patch-attention. We investigate the impact of patch-attention used in the PAC block. The results are shown in Table 5. We examine two conditions. 'MLP' is a no-attention baseline that replaces patch-attention with a pointwise MLP. 'EdgeConv' is a more advanced no-attention baseline that replaces patch-attention with a pointwise MLP followed by max pooling within each kNN neighborhood: this performs feature transformation at each point and enables each point to exchange information with its local neighborhood, but does not leverage attention mechanisms. We can see that patch-attention is more effective than the no-attention baselines. The performance gap between patch-attention and MLP baselines is significant: 93.62% vs. 92.62% and 86.72% vs. 85.32%, an improvement of 1.0 and 1.4 absolute percentage points. Compare with EdgeConv baseline, our patch attention also achieves improvements of 0.52 and 0.83 absolute percentage points.

Effect of 3D Relative position bias. Finally, we investigate the effect of 3D relative position bias used in the MAS block. Table 5 shows results. We can see that the PatchFormer with relative position bias yields +0.47% OA/+0.47% mIoU on ModelNet40 and ShapeNe in relation to those without position encoding respectively, indicating the effectiveness of the relative position bias.

6. Conclusion and Future Work

In this work, we propose a new type of attention mechanism, namely patch-attention for 3D deep learning, which computes a more representative basis set by executing as the K-Means algorithm. The resulting output of patch attention is low-rank and achieves linear complexity to input size. Further, we propose a multi-scale embedding block, building attentions among features of different scales. Experiments show that PatchFormer achieves better accuracy and speed than other 3D Transformers on several representative 3D vision tasks.

We hope that our work will provide empirical guidelines for new method design and inspire further investigation of the properties of 3D Transformers, the development of new

operators and the application of Transformers to other tasks, such as point cloud generation and completion.

7. Acknowledgements

This work was partially supported by the Zhejiang Provincial Natural Science Foundation of China (LGF21F20012), the National Natural Science Foundation of China (No.61602139), and the Graduate Scientific Research Foundation of Hangzhou Dianzi University (CXJJ2021082, CXJJ2021083).

References

- [1] I. Armeni, S. Sax, A. R. Zamir, and S. Savarese. Joint 2d-3d-semantic data for indoor scene understanding. *arXiv preprint arXiv:1702.01105*, 2017. 7
- [2] C. Chen, Q. Fan, and R. Panda. Crossvit: Cross-attention multi-scale vision transformer for image classification. *in ICCV*, 2021. 2
- [3] C. Choy, J. Y. Gwak, and S. Savarese. 4d spatio-temporal convnets: Minkowski convolutional neural networks. *in CVPR*, 2019. 7, 8
- [4] Z. Dai, Z. Yang, Y. Yang, J. G. Carbonell, Q. V. Le, and R. Salakhutdinov. Transformer-xl: Attentive language models beyond a fixed-length context. *in ACL*, 2019. 2
- [5] J. Devlin, M. W. Chang, K. Lee, and K. Toutanova. Bert: Pre-training of deep bidirectional transformers for language understanding. *in NAACL-HLT*, 2018. 1
- [6] A. Dosovitskiy, L. Beyer, A. Kolesnikov, D. Weissenborn, X. Zhai, T. Unterthiner, M. Dehghani, M. Minderer, G. Heigold, S. Gelly, J. Uszkoreit, and N. Houlsby. An image is worth 16x16 words: Transformers for image recognition at scale. *in ICLR*, 2021. 1, 2, 3
- [7] N. Engel, V. Belagiannis, and K. Dietmayer. Point transformer. *CoRR*, abs/2011.00931, 2020. 1, 2, 6
- [8] M.-H. Guo, J.-X. Cai, Z.-N. Liu, T.-J. Mu, R. R. Martin, and S.-M. Hu. Pct: Point cloud transformer. *Computational Visual Media*, 7(2):187–199, Apr 2021. 1, 2, 5, 6
- [9] A. G. Howard, M. Zhu, B. Chen, D. Kalenichenko, W. Wang, T. Weyand, M. Andreetto, and H. Adam. Mobilenets: Efficient convolutional neural networks for mobile vision applications. *arXiv preprint arXiv:1704.04861*, 2017. 2
- [10] Q. Huang, W. Wang, and U. a. Neumann. Recurrent slice networks for 3d segmentation of point clouds. *2018 IEEE/CVF Conference on Computer Vision and Pattern Recognition*, 2018. 2
- [11] T. Le and D. Ye. Pointgrid: A deep network for 3d shape understanding. *in CVPR*, 2018. 6
- [12] J. Lee, W. Yoon, S. Kim, D. Kim, S. Kim, C. H. So, and J. Kang. Biobert: a pre-trained biomedical language representation model for biomedical text mining. *in Bioinformatics*, pages 1234–1240, 2020. 2
- [13] J. Li, B. M. Chen, and G. H. Lee. So-net: Self-organizing network for point cloud analysis. *in CVPR*, 2018. 6
- [14] X. Li, Z. Zhong, J. Wu, Y. Yang, and H. Liu. Expectation-maximization attention networks for semantic segmentation. *in ICCV*, 2019. 1
- [15] Y. Li, R. Bu, M. Sun, and B. Chen. Pointcnn: Convolution on x-transformed points. *Advances in Neural Information Processing Systems (NIPS)*, 2018. 6
- [16] Y. Li, V. G. Kim, D. Ceylan, I. C. Shen, M. Yan, S. Hao, C. Lu, Q. Huang, A. Sheffer, and L. Guibas. A scalable active framework for region annotation in 3d shape collections. *ACM Transactions on Graphics (TOG)*, 35(6cd):210.1–210.12, 2016. 6
- [17] X. Liu, Z. Han, Y. S. Liu, and M. Zwicker. Point2sequence: Learning the shape representation of 3d point clouds with an attention-based sequence to sequence network. *in AAAI*, 2018. 7
- [18] Y. Liu, B. Fan, S. Xiang, and C. Pan. Relation-shape convolutional neural network for point cloud analysis. *in CVPR*, 2019. 7
- [19] Z. Liu, Y. Lin, Y. Cao, H. Hu, Y. Wei, Z. Zhang, S. Lin, and B. Guo. Swin transformer: Hierarchical vision transformer using shifted windows. *arXiv preprint arXiv:2103.14030*, 2021. 1, 2, 5
- [20] Z. Liu, J. Ning, Y. Cao, Y. Wei, Z. Zhang, S. Lin, and H. Hu. Video swin transformer. *CoRR*, abs/2106.13230, 2021. 5
- [21] Z. Liu, H. Tang, Y. Lin, and S. Han. Point-voxel cnn for efficient 3d deep learning. *Advances in Neural Information Processing Systems (NIPS)*, 2019. 2, 6
- [22] K. Mazur and V. Lempitsky. Cloud transformers. *in CVPR*, 2020. 1
- [23] C. R. Qi, H. Su, K. Mo, and L. J. Guibas. Pointnet: Deep learning on point sets for 3d classification and segmentation. *in CVPR*, pages 652–660, 2017. 2, 6, 7
- [24] C. R. Qi, H. Su, M. Niebner, A. Dai, M. Yan, and L. J. Guibas. Volumetric and multi-view cnns for object classification on 3d data. *in CVPR*, 2016. 2
- [25] C. R. Qi, L. Yi, H. Su, and L. J. Guibas. Pointnet++: Deep hierarchical feature learning on point sets in a metric space. *in NIPS*, 2017. 6, 7
- [26] P. Shaw, J. Uszkoreit, and A. Vaswani. Self-attention with relative position representations. *NAACL*, 2018. 2
- [27] Q. Shi, S. Anwar, and N. Barnes. Semantic segmentation for real point cloud scenes via bilateral augmentation and adaptive fusion. *in CVPR*, 2021. 2
- [28] S. Shi, C. Guo, L. Jiang, Z. Wang, J. Shi, X. Wang, and H. Li. Pv-rcnn: Point-voxel feature set abstraction for 3d object detection. *in CVPR*, 2019. 2
- [29] H. Thomas, C. R. Qi, J. E. Deschard, B. Marcotegui, and L. J. Guibas. Kpconv: Flexible and deformable convolution for point clouds. *ICCV*, 2019. 6, 7, 8
- [30] A. Vaswani, P. Ramachandran, A. Srinivas, N. Parmar, B. Hechtman, and J. Shlens. Scaling local self-attention for parameter efficient visual backbones. *in CVPR*, pages 12894–12904, 2021. 1, 5
- [31] A. Vaswani, N. Shazeer, N. Parmar, J. Uszkoreit, L. Jones, A. N. Gomez, L. Kaiser, and I. Polosukhin. Attention is all you need. *in NIPS*, 2017. 1, 2, 3
- [32] L. Wang, Y. Huang, Y. Hou, S. Zhang, and J. Shan. Graph attention convolution for point cloud semantic segmentation. *2019 IEEE/CVF Conference on Computer Vision and Pattern Recognition (CVPR)*, 2019. 2

- [33] P. Wang, Y. Yang, Q. Zou, Z. Wu, Y. Liu, and X. Tong. Un-supervised 3d learning for shape analysis via multiresolution instance discrimination. *in AAAI*, pages 2773–2781, 2021. [4](#)
- [34] W. Wang, E. Xie, X. Li, D. Fan, K. Song, D. Liang, T. Lu, P. Luo, and L. Shao. Pyramid vision transformer: A versatile backbone for dense prediction without convolutions. *in ICCV*, 2021. [1](#), [2](#), [5](#), [6](#), [7](#), [8](#)
- [35] W. Wang, L. Yao, L. Chen, D. Cai, X. He, and W. Liu. Cross-former: A versatile vision transformer based on cross-scale attention. *in NIPS*, 2021. [1](#), [2](#), [5](#)
- [36] Y. Wang, Y. Sun, Z. Liu, S. E. Sarma, M. M. Bronstein, and J. M. Solomon. Dynamic graph cnn for learning on point clouds. *ACM Transactions on Graphics*, 38(5), 2018. [2](#), [6](#), [7](#)
- [37] Z. Wang and F. Lu. Voxsegnet: Volumetric cnns for semantic part segmentation of 3d shapes. *IEEE Transactions on Visualization and Computer Graphics*, pages 1–1, 2019. [2](#)
- [38] K. Wu, H. Peng, M. Chen, J. Fu, and H. Chao. Rethinking and improving relative position encoding for vision transformer. *in ICCV*, 2021. [5](#)
- [39] Z. Wu, S. Song, A. Khosla, X. Tang, and J. Xiao. 3d shapenets for 2.5d object recognition and next-best-view prediction. *in CVPR*, 2014. [6](#)
- [40] Z. Wu, S. Song, A. Khosla, F. Yu, L. Zhang, X. Tang, and J. Xiao. 3d shapenets: A deep representation for volumetric shapes. *2015 IEEE Conference on Computer Vision and Pattern Recognition (CVPR)*, 2015. [6](#)
- [41] Y. Xu, T. Fan, M. Xu, Z. Long, and Q. Yu. Spidercnn: Deep learning on point sets with parameterized convolutional filters. *ECCV*, 2018. [6](#)
- [42] X. Yan, C. Zheng, Z. Li, S. Wang, and S. Cui. Pointasnl: Robust point clouds processing using nonlocal neural networks with adaptive sampling. *2020 IEEE/CVF Conference on Computer Vision and Pattern Recognition (CVPR)*, 2020. [6](#), [7](#), [8](#)
- [43] B. Yang, J. Wang, R. Clark, Q. Hu, S. Wang, A. Markham, and N. Trigoni. Learning object bounding boxes for 3d instance segmentation on point clouds. *2019 IEEE/CVF Conference on Computer Vision and Pattern Recognition (CVPR)*, 2019. [2](#)
- [44] Z. Yang, Z. Dai, Y. Yang, J. Carbonell, R. R. Salakhutdinov, and Q. V. Le. Xlnet: Generalized autoregressive pretraining for language understanding. *in NIPS*, 32, 2019. [2](#)
- [45] C. Zhang, H. Wan, S. Liu, X. Shen, and Z. Wu. Pvt: Point-voxel transformer for 3d deep learning. *CoRR*, abs/2108.06076, 2021. [2](#)
- [46] F. Zhang, Y. Chen, Z. Li, Z. Hong, J. Liu, F. Ma, J. Han, and E. Ding. Acfnnet: Attentional class feature network for semantic segmentation. *in ICCV*, 2019. [1](#)
- [47] K. Zhang, M. Hao, J. Wang, C. D. Silva, and C. Fu. Linked dynamic graph cnn: Learning on point cloud via linking hierarchical features. *arXiv:1904.10014 [cs]*, 2019. [2](#), [6](#)
- [48] H. Zhao, L. Jiang, C. W. Fu, and J. Jia. Pointweb: Enhancing local neighborhood features for point cloud processing. *2019 IEEE/CVF Conference on Computer Vision and Pattern Recognition (CVPR)*, 2019. [2](#)
- [49] H. Zhao, L. Jiang, C.-W. Fu, and J. Jia. Pointweb: Enhancing local neighborhood features for point cloud processing. *Proceedings of the IEEE/CVF Conference on Computer Vision and Pattern Recognition*, pages 5565–5573, 2019. [6](#)
- [50] H. Zhao, L. Jiang, J. Jia, P. Torr, and V. Koltun. Point transformer. *in ICCV*, 2021. [1](#), [6](#)
- [51] Y. Zhou and O. Tuzel. Voxnet: End-to-end learning for point cloud based 3d object detection. *in ICCV*, pages 4490–4499, 2018. [2](#)